Electronic Supplementary Material (ESI) for Journal of Materials Chemistry B.
This journal is © The Royal Society of Chemistry 2021

Supplementary information

Tumor Microenvironment-responsive multifunctional nanoplatform Based on $MnFe_2O_4$-PEG for Enhanced Magnetic Resonance Imaging-guided Hypoxic Cancer Radiotherapy

Zhenhu He,[a,b] Haixiong Yan,[a,b] Wenbin Zeng,[d] Kai Yang,[e] Pengfei Rong*[a,b,c]

a. Department of Radiology, the Third Xiangya Hospital, Central South University, Changsha, Hunan 410013, China.

b. Molecular Imaging Research Center, Central South University, Changsha, Hunan 410013, China.

c. Key Laboratory of Biological Nanotechnology of National Health Commission, Changsha, Hunan 410008, China

d. Xiangya School of Pharmaceutical Sciences, Central South University, Changsha, Hunan 410013, China.

e. School of Radiation Medicine and Protection and School for Radiological and Interdisciplinary Sciences (RAD-X), Collaborative Innovation Center of Radiation Medicine of Jiangsu Higher Education Institutions Medical College of Soochow University, Suzhou, Jiangsu 215123, China.

Corresponding author E-mail: rongpengfei66@163.com

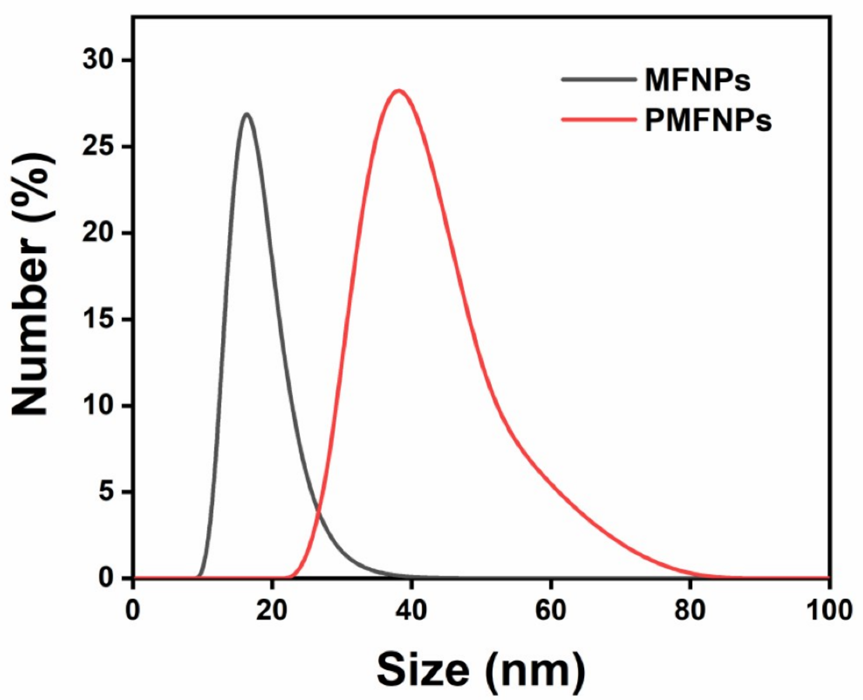

Figure S1. Dynamic light scattering (DLS) data of $MnFe_2O_4$ in n-Hexane and $MnFe_2O_4$-PEG in deionized water.

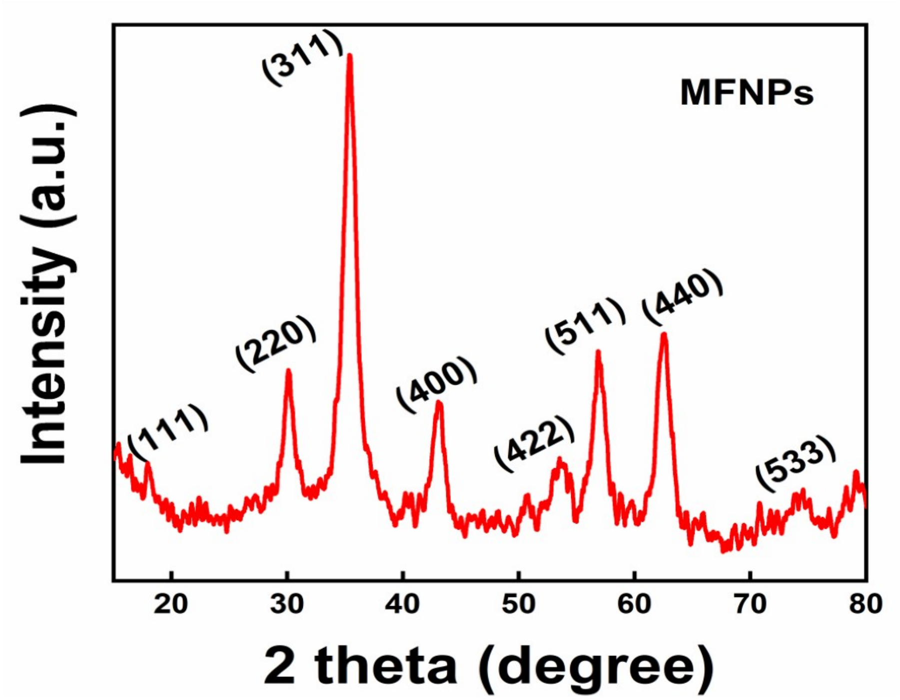

Figure S2. X-ray powder diffraction (XRD) patterns of $MnFe_2O_4$.

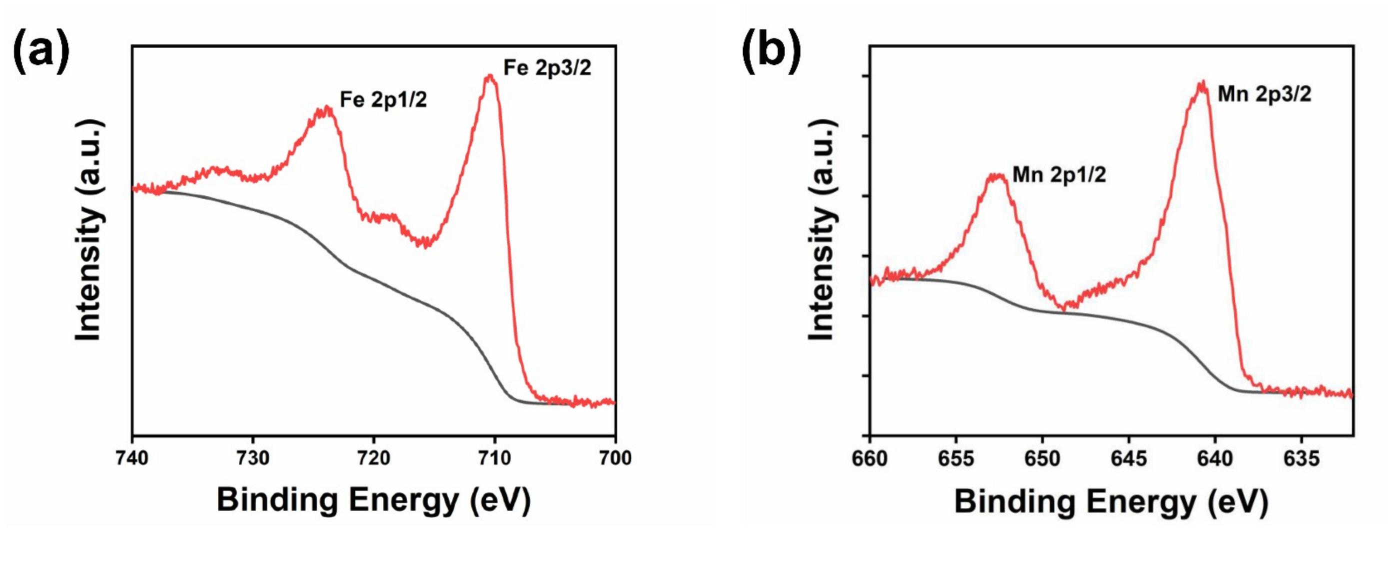

Figure S3. X-ray photoelectron spectroscopy (XPS) of $MnFe_2O_4$: (a) Fe 2p. (b) Mn 2p. The Fe 2p3/2 peak observed at 711.3 eV, and Mn 2p3/2 peak observed at 640.9 eV correspond to Fe^{3+} and Mn^{2+} species, respectively.

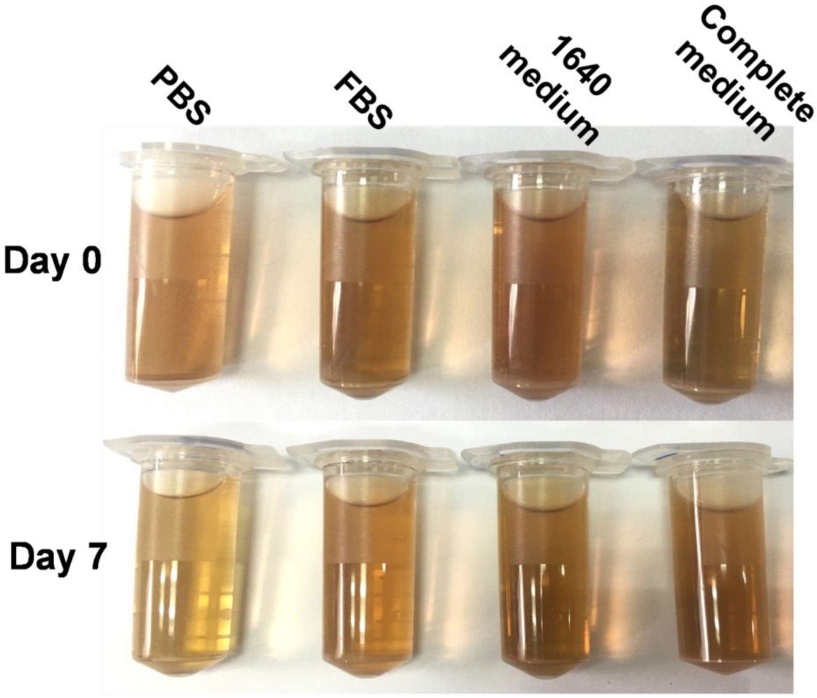

Figure S4. The stability of $MnFe_2O_4$-PEG in PBS, FBS, 1640 medium, and complete medium. The photos were taken on day 0 and day 7, respectively.

$$\mathbf{Mn^{2+} + H_2O_2 \rightarrow 2H^+ + MnO_2} \quad \textbf{(1)}$$

$$\mathbf{MnO_2 + H_2O_2 + 2H^+ \rightarrow Mn^{2+} + 2H_2O + O_2 \uparrow} \quad \textbf{(2)}$$

$$\mathbf{Fe^{3+} + H_2O_2 \rightarrow Fe^{2+} + HOO\cdot + H^+} \quad \textbf{(3)}$$

$$\mathbf{Fe^{3+} + HOO\cdot \rightarrow Fe^{2+} + H^+ + O_2 \uparrow} \quad \textbf{(4)}$$

$$\mathbf{Fe^{2+} + H_2O_2 \rightarrow Fe^{3+} + OH^- + OH\cdot} \quad \textbf{(5)}$$

Figure S5. Reaction equations (1) and (2): Mechanism of catalyzing hydrogen peroxide to produce oxygen by Mn^{2+}. Reaction equations (3), (4), and (5): Mechanism of catalyzing hydrogen peroxide to produce hydroxyl radical by Fe^{3+}.

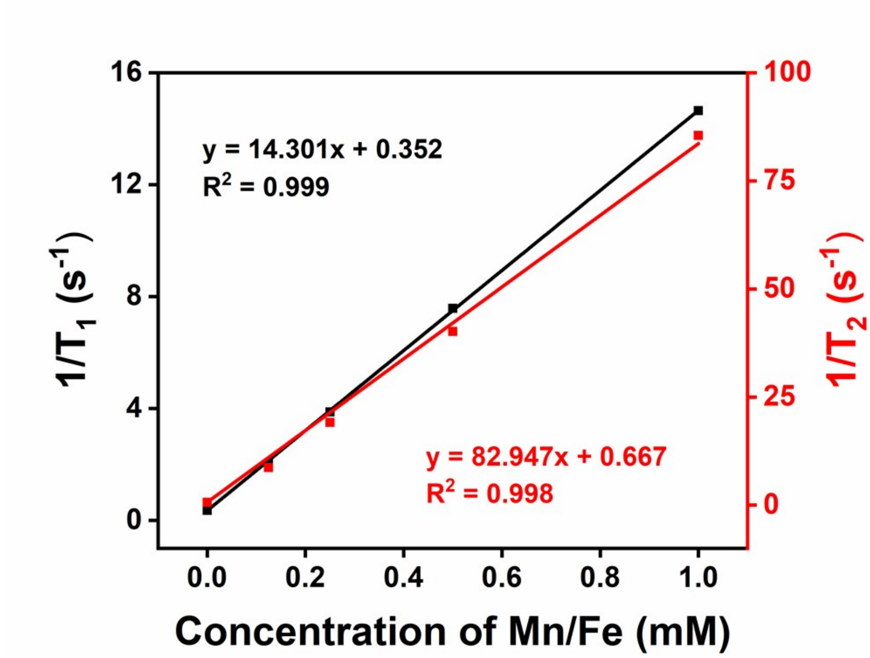

Figure S6. T_1 relaxation rate and T_2 relaxation rate of $MnFe_2O_4$-PEG nanoparticles measured as the function of Mn and Fe concentrations, respectively. r_1 = 14.301 $mM^{-1}s^{-1}$, r_2 = 82.947 $mM^{-1}s^{-1}$. Scanned by a Bruker Minispec analyzer (60 MHz).

$Fe^{3+} + GSH \rightarrow Fe^{2+} + GSSG$ （1）[1]

$Fe^{2+} + H_2O_2 \rightarrow Fe^{3+} + OH^{-} + OH\cdot$ （2）

$MnO_2 + 2\ GSH + 2\ H^{+} \rightarrow Mn^{2+} + GSSG + 2\ H_2O$ （3）[2]

$Mn^{2+} + H_2O_2 \rightarrow MnO_2 + 2\ H^{+}$ （4）

Figure S7. Reaction equations of GSH consumption.

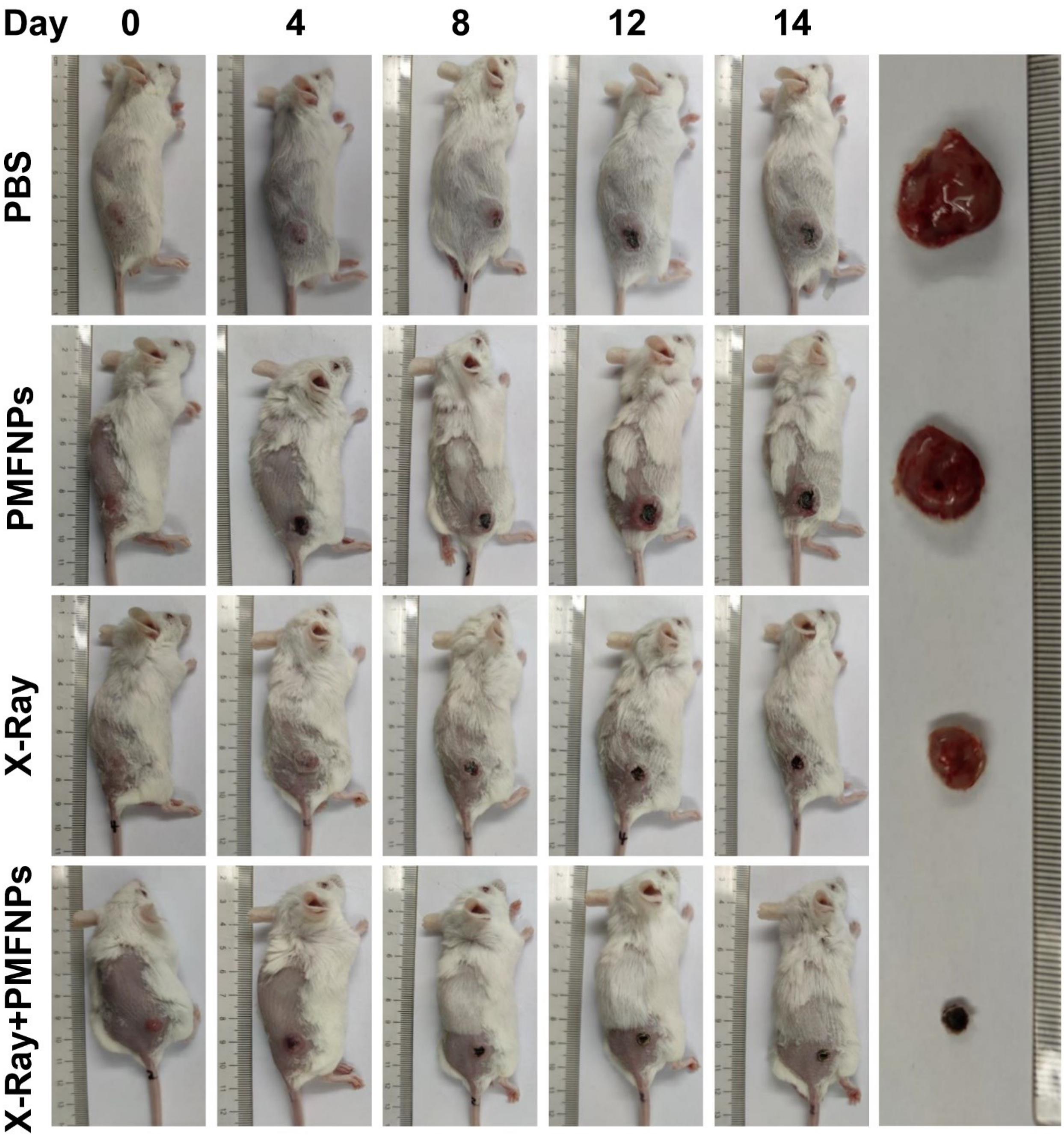

Figure S8. Digital photograph of mice bearing tumor. The tumor in the X-Ray + PMFNPs group has been necrotic and scabby.

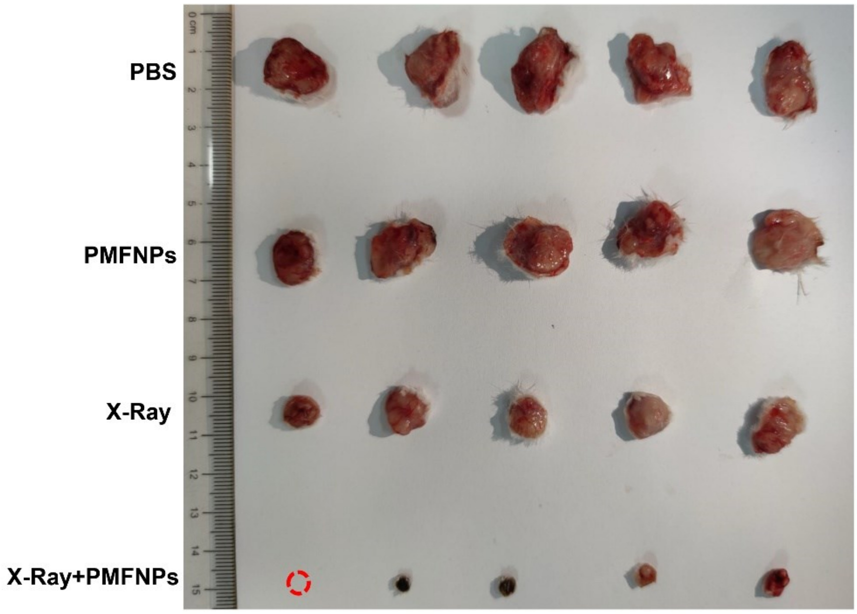

Figure S9. Digital photograph of the tumors.

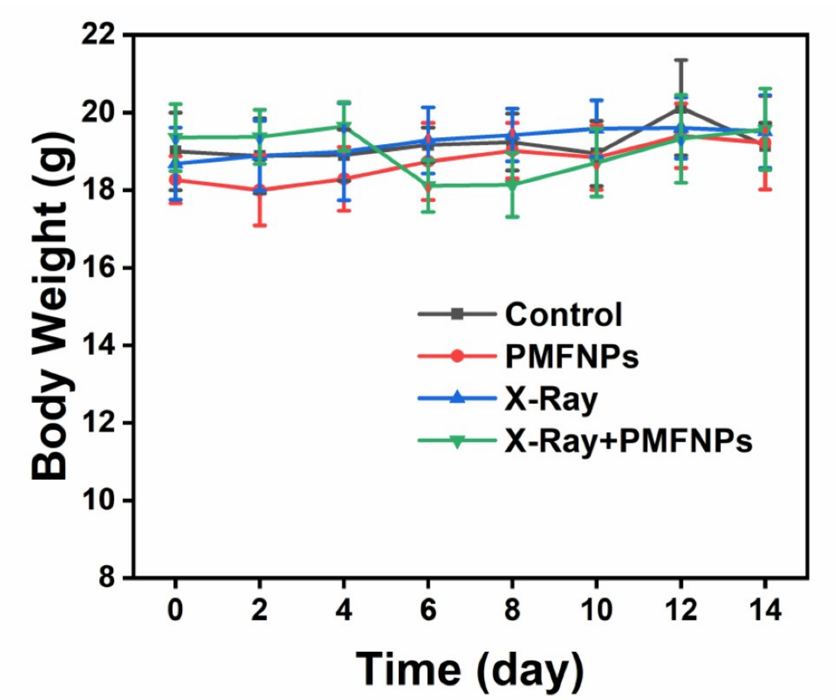

Figure S10. The body weight curves of mice after various treatments during the observation period (n = 5).

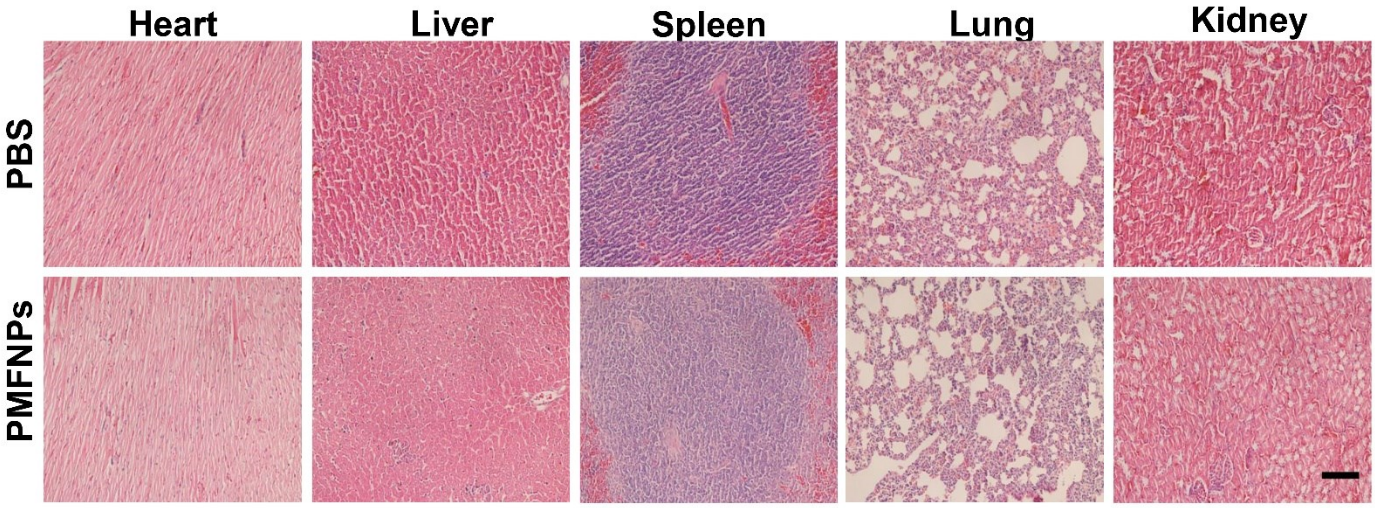

Figure S11. Hematoxylin-eosin (H&E) stainings images of main organs from different treatment groups (scale bar:100 µm).

Reference

1. X. Wan, L. Song, W. Pan, H. Zhong, N. Li and B. Tang, *ACS Nano*, 2020, **14**, 11017-11028.
2. Z. Z. Dong, L. Lu, C. N. Ko, C. Yang, S. Li, M. Y. Lee, C. H. Leung and D. L. Ma, *Nanoscale*, 2017, **9**, 4677-4682.